

Evaluating the added benefit of CT texture analysis on conventional CT analysis to differentiate benign ovarian cysts

Minkook Seo 
Moon Hyung Choi 
Young Joon Lee 
Seung Eun Jung 
Sung Eun Rha 

PURPOSE

We aimed to evaluate the benefit of adding CT texture analysis on conventional CT features of benign adnexal cystic lesions, especially in identifying mucinous cystadenoma.

METHODS

This retrospective study included patients who underwent surgical removal of benign ovarian cysts (44 mucinous cystadenomas, 32 serous cystadenomas, 16 follicular/simple cysts and 43 endometriotic cysts) at our institution between January 2015 and November 2017. The CT images were independently reviewed by an abdominal radiologist (reviewer 1) and a resident (reviewer 2). Both reviewers recorded the conventional characteristics and performed texture analysis. Based on reviewer 1's results, two decision trees for differential diagnosis were developed. Reviewer 2's results were then applied to the decision trees. The diagnostic performances of each reviewer with and without the decision trees were compared.

RESULTS

Several conventional features and texture analysis parameters showed significant differences between mucinous cystadenomas and other benign adnexal cysts. The first decision tree selected septum number and thickness as significant features, whereas the second decision tree selected septum number and the mean values at spatial scaling factor (SSF) 0. Reviewer 1's performance did not change significantly with or without the use of the decision trees. Reviewer 2's interpretations were significantly less sensitive than reviewer 1's interpretations ($p = 0.001$). However, when aided by the first and second decision trees, Reviewer 2's interpretations were significantly more sensitive than reviewer 1's interpretations (86.4%, $p < 0.001$; 72.7%, $p = 0.001$).

CONCLUSION

This study suggests the benefit of CT texture analysis on conventional images to differentiate mucinous cystadenoma from other benign adnexal cysts, particularly for less experienced radiologists.

In the assessment of a possible adnexal mass, it is paramount to differentiate benign lesions from malignancies, since their treatment strategies and prognoses drastically differ (1). Approaches to the lesions can even vary among different benign masses. Simple or follicular cysts do not require surgery at all, whereas epithelial tumors need to be resected for pathologic confirmation of their benignity and relief of the symptoms caused by mass effects. The treatment plan for endometriotic cysts varies based on the extent and severity of symptoms.

Ultrasonography (US) is often the first imaging method performed in the evaluation of an ovarian lesion because it is widely available, well accepted by the patients, noninvasive and inexpensive (2). Magnetic resonance imaging (MRI) is an essential problem solving tool for characterizing an US-indeterminate adnexal mass, owing to its high resolution with excellent soft tissue contrast, possessing proven superiority over other modalities (1–4). Computed tomography (CT) is generally not intended for primary pelvic or gynecologic evaluation in women, unlike US or MRI (5). Its value in tumor characterization is limited by the detection of fat or calcifications within the lesion and the assessment of its rough shape, which may, but not necessarily, lead to a specific diagnosis (2, 3). In contrast to its suboptimal

From the Department of Radiology (M.S., S.E.R.) Seoul St. Mary's Hospital, College of Medicine, the Catholic University of Korea, Seoul, Republic of Korea; Department of Radiology (M.H.C. ✉ cmh@catholic.ac.kr, Y.J.L., S.E.J.) and Catholic Smart Imaging Center (M.H.C., S.E.J.), Eunpyeong St. Mary's Hospital, College of Medicine, the Catholic University of Korea, Seoul, Republic of Korea.

Received 10 April 2020; revision requested 17 May 2020; last revision received 3 July 2020; accepted 24 July 2020.

Published online 28 June 2021.

DOI 10.5152/dir.2021.20225

You may cite this article as: Seo M, Choi MH, Lee YJ, Jung SE, Rha SE. Evaluating the added benefit of CT texture analysis on conventional CT analysis to differentiate benign ovarian cysts. *Diagn Interv Radiol* 2021; 27:460-468

diagnostic value, recent widespread use of CT has commonly resulted in the incidental initial detection of an adnexal lesion (4–7).

Common benign adnexal cystic lesions include functional cysts, serous cystadenomas, mucinous cystadenomas, and endometriotic cysts. Mucinous cystadenomas are characterized as multilocular cystic adnexal masses with variable internal mucinous contents and relatively large size at the time of presentation (2, 3, 8). As with most ovarian masses, it is challenging to make a specific diagnosis of mucinous cystadenoma and exclude other pathologic types, particularly when either US or CT is the only available modality. Two prior studies reported that the detection rates for mucinous cystadenoma using US, CT, and MRI were 50%, 62%, and 70%, respectively (9, 10). On MRI, mucinous tumors classically have a “stained glass appearance” with variable intralocular signal intensities, which allows a more specific differential diagnosis from other tumors than is possible with US and CT (2, 11). However, MRI is too costly and time-consuming to be performed routinely for incidentally found benign diseases.

Recent advances in endoscopic surgical techniques have offered new possibilities for the laparoscopic treatment of large ovarian cysts, including mucinous cystadenomas, rather than laparotomy (12). The fluid content of a large cyst must be aspirated before it can be laparoscopically excised and removed (12). However, thick internal materials such as mucin or fat may impair this procedure. One reported case of laparoscopy had to be converted to open laparotomy due to an inability to aspirate the cyst’s liquid contents (13). The laparoscopic removal of large mucinous cystadenomas also poses the risk of spillage, which can cause pseudomyxoma peritonei (14–16).

Therefore, it would be helpful to properly analyze the cyst’s internal contents and correctly preoperatively characterize the nature of the lesion to plan the surgery and avoid complications. Because of the limited availability of MRI, we evaluated the utility of CT with added texture analysis to differentiate the internal mucinous contents of ovarian cysts from serous fluid and eventually predict the pathologic diagnosis of the adnexal cystic lesion. Texture analysis is a method used to quantitatively evaluate pixel densities in medical images. Although texture analysis had been used in some previous studies on ovarian cancers, no study has performed texture analysis in ovarian cysts (17–19).

Consequently, the purpose of this study is to evaluate the benefit of adding CT texture analysis to conventional CT features when diagnosing benign adnexal cystic lesions, and especially when identifying mucinous cystadenoma.

Methods

This retrospective study was approved by our Institutional Review Board (KC18RESI0292). Informed consent from the enrolled patients was waived given its retrospective nature.

Using the electrical medical record database from our tertiary care institution, we identified patients who underwent gynecologic surgeries to remove benign ovarian cysts between January 2015 and November 2017. A total of 437 patients underwent such surgeries. Mucinous cystadenomas, serous cystadenomas, follicular or simple cysts and endometriotic cysts were confirmed in 130, 88, 66, and 153 patients, respectively. Among them, we only included patients who had preoperative contrast-enhanced CT imaging, including portal phase imaging, within 60 days of surgery. Fig. 1 shows the flow diagram for patient selection.

Some patients underwent CT at our institution, while others underwent CT as outpatients. Intra-institutional CT was performed using 128-channel CT scanners (Discovery CT750, GE Healthcare; Somatom Definition or Definition AS+, Siemens Healthineers). Images were acquired helically at 80–120 kVp and 248–578 reference mAs under automatic exposure control with 5 mm thickness and no gap. Approximately 110 mL of nonionic iodine-based intravenous contrast material (iopromide, Ultravist®, Bayer AG or iohexol, Iobrix 300®, Accuzen) was injected, followed by a 20 mL saline flush.

Main points

- Among conventional CT features, septum number and thickness were considered as significant for differentiation of mucinous cystadenomas from other benign ovarian cysts.
- Among CT texture analysis parameters, mean value (SSF0) was considered to be significant.
- Based on our two decision tree models, the addition of texture analysis to conventional image analysis is helpful to differentiate mucinous cystadenoma from other benign adnexal cysts, particularly for less experienced radiologists.

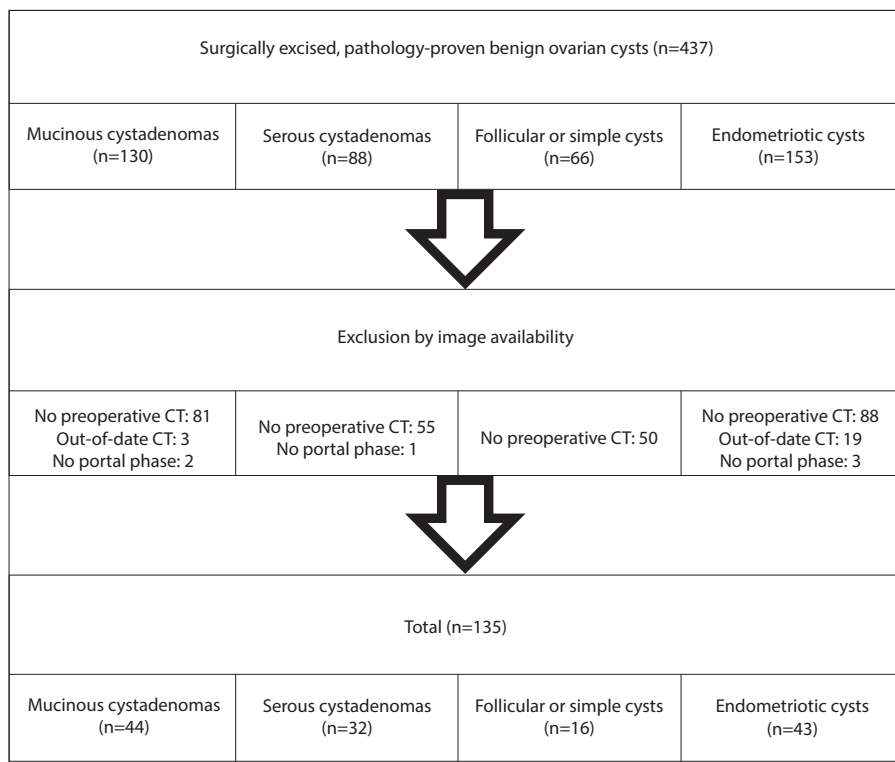


Figure 1. A flow diagram showing the process of patient selection. Out-of-date CT refers to a preoperative CT that was performed >60 days before the surgery.

The imaging acquisition parameters may have been different for the patients who underwent CT imaging at outside facilities. However, an abdominal radiologist assured that all CTs performed for outpatients were of proper image quality before the images were reviewed.

Two reviewers independently evaluated the images of the ovarian cysts using a picture archiving and communication system. Reviewer 1 is a specialist of abdominal imaging with 9 years of experience and reviewer 2 is a resident. The reviewers were blinded to the patients' pathologic diagnoses. They recorded conventional characteristics of the ovarian cysts and performed texture analysis. Conventional image analysis consisted of qualitative and quantitative analysis. Qualitative characteristics included: lesion internal homogeneity, margins, number of locules, thickness of the walls and septa, presence of calcifications and bilaterality. Quantitative characteristics included: axial and coronal diameters, and the densities of most hyperdense and hypodense areas in the cyst. The characteristics used in this study were based on previous studies attempting to differentiate tumor types among benign adnexal lesions using conventional CT features (11, 20, 21).

The cysts were considered multilocular when they had two or more locules. The walls and septa were considered "thick" when most of them were prominently visible. The internal homogeneity was determined by visual assessment, which was independent of the quantitatively measured density. Lesions were characterized as bilateral if there was another lesion that was >2 cm in size with similar characteristics on the contralateral ovary. Lesion margins were determined by the outer contours and overall shapes of the locules. Lesions with regularly smooth and round contours were considered to have smooth margins, and lesions with lobulated contours and relatively uniform oval locules were considered to have lobulated margins. Lesions with irregular contours and variably shaped (i.e., mixed oval and tubular) locules were considered to have pleomorphic margins. Based on the characteristics of each cyst, the reviewers determined the most likely diagnosis of the ovarian cysts, and the diagnosis was called the radiologist's interpretation.

The two reviewers independently performed texture analysis by using commercial software (TexRAD, TexRAD Ltd.). The reviewers selected the single axial image that

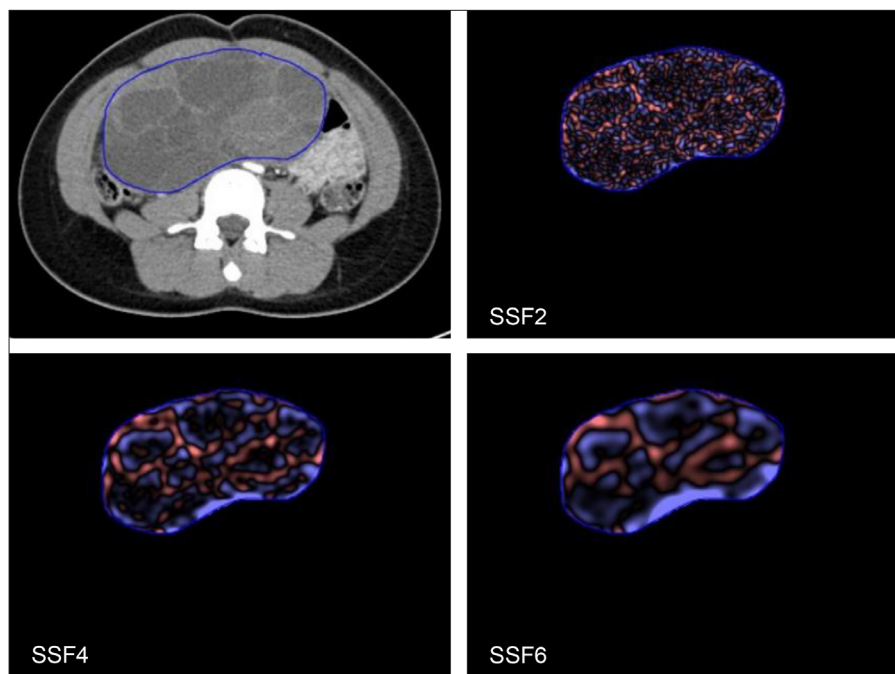


Figure 2. An example of texture analysis of ovary cyst (pathologically confirmed mucinous cystadenoma) using different filter levels (spatial scaling factors 2, 4, and 6).

most completely demonstrated the lesion's complexity. They drew regions of interest (ROIs) that covered the entire area of the lesion on the selected axial image using a polygonal ROI tool (Fig. 2). The spatial scaling factor (SSF) was set between 0 and 6, representing fine to coarse texture. We then obtained the histogram of pixel attenuation values included in the ROI. Its characteristics included mean attenuation, standard deviation (SD), entropy (irregularity of the value distribution), mean of positive pixels (MPP), skewness (asymmetry of the histogram), and kurtosis (peakedness of the histogram).

Statistical analysis

Patient age at the time of presentation was compared between each diagnosis using an independent t-test. For the qualitative characteristics from the conventional image analysis, the interobserver variability was evaluated using kappa statistics. The frequency of quantitative characteristics was compared among the diagnoses using the chi-square test. The normality of the distributions was tested by Kolmogorov-Smirnov tests for the quantitative parameters of the conventional image analysis and texture analysis. As many parameters were not normally distributed, differences in the quantitative parameters among the four diagnoses were compared using the Kruskal-Wallis test and Mann-Whitney U test.

We developed two decision tree models for the differential diagnosis of ovarian cysts. The decision tree models were developed using recursive partitioning analysis based on 1) the conventional image analysis and 2) the conventional image and texture analyses performed by reviewer 1. The variables that were significantly different among the four pathologic diagnoses were examined in the recursive partitioning. Recursive partitioning determines a cutoff point that can differentiate all ovarian cysts by pathology and selects variables with the best performance. To classify the ovarian cysts, the results of reviewer 2's image analysis were then applied to the two decision trees derived from reviewer 1's results. The diagnostic performance was compared with the dichotomized pathology categorization (mucinous cystadenoma versus others). The diagnostic performance of the two radiologists' interpretations and diagnoses from the decision tree was reported as the sensitivity, specificity, positive predictive value, negative predictive value, and accuracy. The sensitivity and specificity of the diagnostic methods were compared using McNemar test.

The statistical analysis was performed using SPSS Statistics 24.0 (IBM Corporation) and R version 3.2.3 (<https://www.R-project.org>) (22). *p* values <0.05 were considered statistically significant.

Table 1. Conventional image analysis by both reviewers regarding qualitative radiologic features and inter-reader agreement

		Reviewer 1					Reviewer 2					<i>p</i>	κ	<i>p</i>
		Simple or follicular cyst (n=16)	Serous cyst-adenoma (n=32)	Mucinous cyst-adenoma (n=44)	Endo-metriotic cyst (n=43)	<i>p</i>	Simple or follicular cyst (n=16)	Serous cyst-adenoma (n=32)	Mucinous cyst-adenoma (n=44)	Endo-metriotic cyst (n=43)				
Cyst wall	Thin	15	31	41	32	0.009	10	16	12	4	<0.001	0.091	0.022	
	Thick	1	1	3	11	6	16	32	39					
Septum number	0	11	16	7	22	<0.001	9	16	1	13	<0.001	0.498	<0.001	
	1	2	4	1	10		3	6	5	13				
	≥2	3	12	36	11		4	10	38	17				
Septum thickness	No septum	11	16	7	22	<0.001	9	16	1	13	<0.001	0.453	<0.001	
	Thin	0	16	24	11		4	8	9	7				
	Thick	5	0	13	10		3	8	34	23				
Locule number	Unilocular	11	17	7	24	<0.001	9	18	2	13	<0.001	0.456	<0.001	
	Multilocular	5	15	37	19		7	14	42	30				
Homogeneity	Homogeneous	12	27	29	19	0.003	8	24	30	19	0.025	0.560	<0.001	
	Heterogeneous	4	5	15	24		8	8	14	24				
Calcification	Absence	16	31	35	41	0.011	13	23	29	42	0.002	0.258	0.001	
	Presence	0	1	9	2		3	9	15	1				
Bilaterality	Unilateral	15	27	43	29	0.001	14	26	37	26	0.030	0.605	<0.001	
	Bilateral	1	5	1	14		2	6	7	17				
Margin	Smooth	11	19	12	22	0.003	13	20	14	16	<0.001	0.386	<0.001	
	Lobulated	5	13	32	18		2	9	14	21				
	Pleomorphic	0	0	0	3		1	3	16	6				

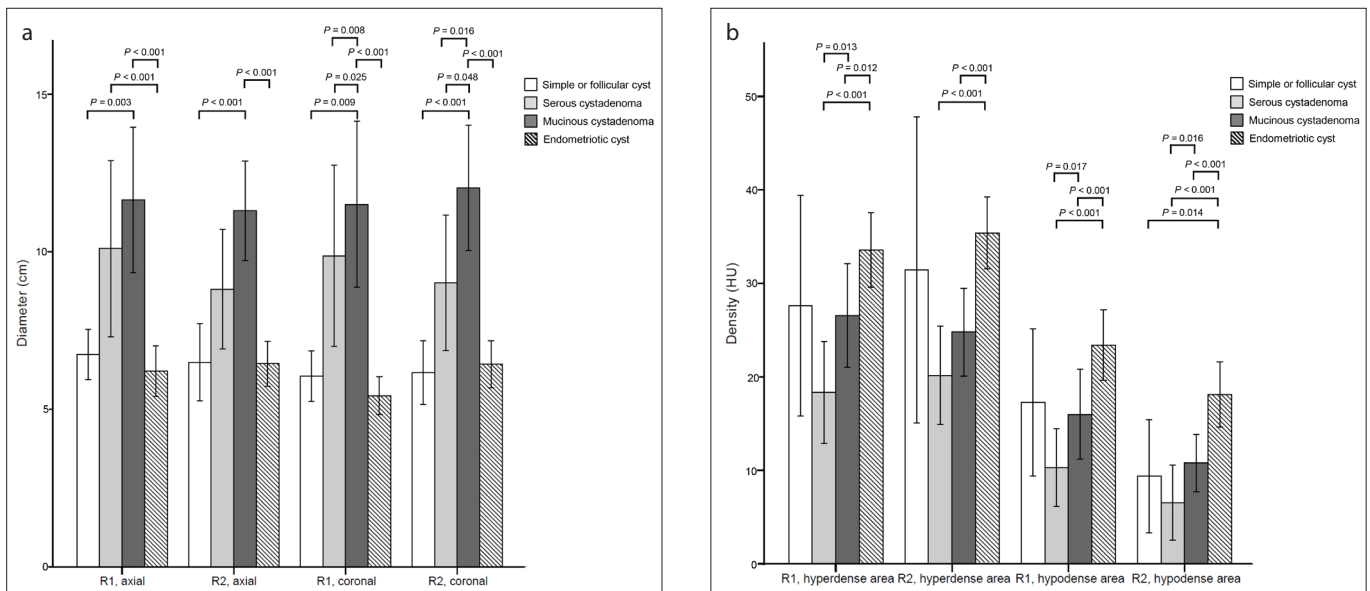


Figure 3. a, b. Comparison of quantitative parameters in conventional analysis by cyst type. Axial and coronal diameters of the ovary cysts measured by two reviewers (a) and the cyst density measured at most hyperdense and most hypodense areas (b). R1, reviewer 1; R2, reviewer 2.

Results

The mean age of patients with follicular/simple cysts, serous cystadenomas, mucinous cystadenomas and endometriotic

cysts were 49.5 ± 15.7 , 57.3 ± 15.8 , 47.3 ± 14.7 , and 33.3 ± 10.6 years, respectively. Patients with endometriotic cysts were significantly younger than patients with follicular/sim-

ple cysts, serous cystadenomas, and mucinous cystadenomas ($p = 0.001$, $p < 0.001$, $p < 0.001$, respectively). In contrast, patients with serous cystadenomas were significant-

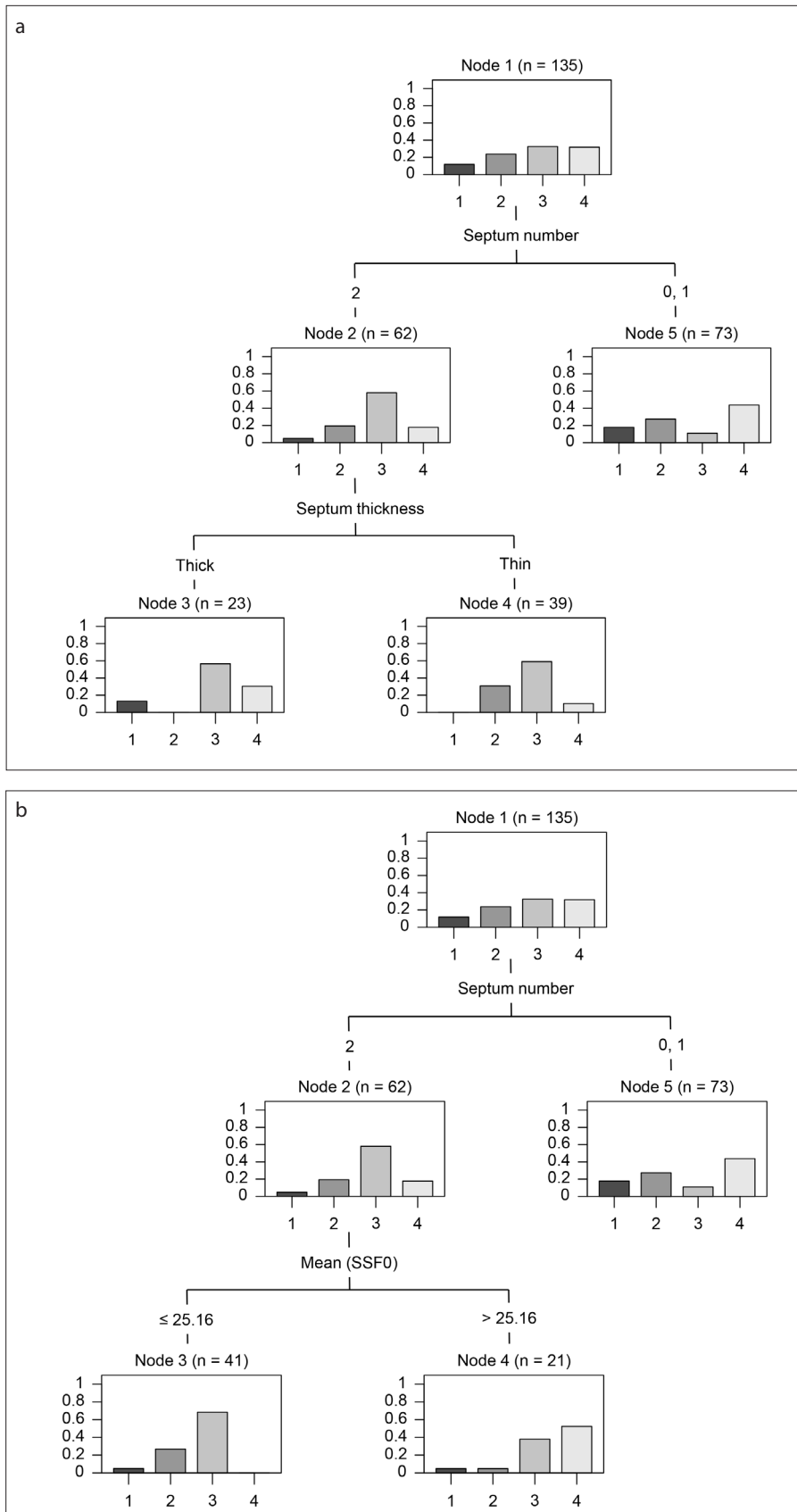


Figure 4. a, b. Decision tree analysis for the diagnosis of ovarian cysts. Decision tree based on reviewer 1's conventional image analysis (a) and decision tree based on reviewer 1's conventional image analysis and texture analysis (b). 1, simple or follicular cysts; 2, serous cystadenomas; 3, mucinous cystadenomas; 4, endometriotic cysts.

ly older than those with mucinous cystadenomas ($p = 0.012$).

The conventional qualitative radiologic findings of the two reviewers and their interobserver agreement are summarized in Table 1. All imaging features were significantly different across the four diagnoses in both reviewers' analyses. Although the kappa statistics revealed significant interobserver agreement, evaluation of the cyst wall had the lowest kappa value. The highest interobserver agreement was found in bilaterality ($\kappa=0.605$). Table 2 shows the differences in the imaging features between mucinous cystadenoma and other cysts. The following imaging features were significantly different between mucinous cystadenomas and other cysts and commonly appeared in both readers' image analysis: septum number, septum thickness, locule number and margin. Many septa, thick septa and many locules were more frequent in mucinous cystadenomas than in other cysts. The axial and coronal diameters of mucinous cystadenomas were significantly larger than those of simple/follicular cysts and endometriotic cysts (Fig. 3a). Endometriotic cysts had the highest density, while serous cystadenomas had the lowest density regardless of whether it was measured at the most hyperdense or the most hypodense area. There were significant differences among serous cystadenomas, mucinous cystadenomas and endometriotic cysts (Fig. 3b). The diagnostic accuracy of reviewer 1 in identifying the four types of ovarian cysts was 52.6% (71/135), while reviewer 2's accuracy was 43.0% (58/135) (Table 3). The sensitivities in diagnosing mucinous cystadenoma were 68.2% and 31.8% from reviewers 1 and 2, respectively.

Many CT texture analysis parameters were significantly different between the four pathologic diagnoses (Table 4). In particular, the mean, SD, and entropy-related parameters were most frequently significantly different between mucinous cystadenomas and other cysts. This difference was particularly true between mucinous cystadenomas and endometriotic cysts. As SSF0 means that no filter was applied in the texture analysis, the mean values at SSF0 of the four cysts were similar to the quantitative measurements from the conventional analysis.

Using the conventional imaging features that were significantly different among the four types of cysts, the septum number and septum thickness were selected as import-

Table 2. Significance (*p* values) of differences in conventional imaging findings between mucinous cystadenomas and other cysts

Mucinous cystadenoma vs.	Reviewer 1			Reviewer 2		
	Simple or follicular cyst	Serous cystadenoma	Endometriotic cyst	Simple or follicular cyst	Serous cystadenoma	Endometriotic cyst
Cyst wall	0.938	0.634	0.021	0.017	0.055	0.051
Septum number	<0.001	<0.001	<0.001	<0.001	<0.001	<0.001
Septum thickness	<0.001	<0.001	0.002	<0.001	<0.001	0.002
Locule number	<0.001	0.001	<0.001	<0.001	<0.001	0.002
Homogeneity	0.754	0.112	0.053	0.234	0.612	0.031
Calcification	0.096	0.038	0.049	0.346	0.625	<0.001
Bilaterality	0.466	0.077	<0.001	0.746	0.766	0.017
Margin	0.006	0.009	0.007	0.003	0.009	0.048

Table 3. Comparison between radiologists' interpretation and pathologic diagnosis

		Pathology			
		Simple or follicular cyst (n = 16)	Serous cystadenoma (n = 32)	Mucinous cystadenoma (n = 44)	Endometriotic cyst (n = 43)
Reviewer 1	Simple or follicular cyst	4	5	1	7
	Serous cystadenoma	7	16	11	5
	Mucinous cystadenoma	3	5	30	10
	Endometriotic cyst	2	6	2	21
Reviewer 2	Simple or follicular cyst	5	7	4	12
	Serous cystadenoma	3	15	24	3
	Mucinous cystadenoma	2	4	14	4
	Endometriotic cyst	6	6	2	24

ant features in the first decision tree. To make the second decision tree, the texture analysis parameters that were significantly different among the four diagnoses were added to the conventional image analysis parameters. The second tree selected the septum number among the conventional parameters and the mean value at SSF0 among the texture analysis parameters. Both decision trees were created based on reviewer 1's analysis. Using the first decision tree based on conventional imaging features, the patients were divided into three groups. The percentages of the four pathologic diagnoses are shown in Fig. 4a. To classify the cysts into the four pathologic categories, Nodes 3 and 4 were used to diagnose mucinous cystadenomas, while Node 5 was used to diagnose endometriotic cysts. The second decision tree also divided the patients into three groups (Fig. 4b). Node 3 was used to diagnose mucinous cystadenomas, while Nodes 4 and 5 were used to diagnose endometriotic cysts. The results of reviewer 2's analyses were then applied to both decision trees.

The sensitivity, specificity, positive predictive value, negative predictive value, and accuracy of the two decision trees (conventional analysis versus conventional and texture analysis) are summarized in Table 5. The results of McNemar tests, which compared the diagnostic performance of reviewer 1's interpretation with those of other methods, are also shown in Table 5. McNemar test showed that there was no significant difference in sensitivity or specificity between reviewer 1's interpretation and the diagnosis based on the decision tree. Without the decision trees, reviewer 2 had a significantly lower sensitivity than reviewer 1. Using the first and the second decision trees, reviewer 2's sensitivity increased to 86.4% and 72.1%, respectively, which were significantly higher than those of reviewer 1's interpretation ($p < 0.001$ and $p = 0.001$, respectively).

Discussion

This study indicates that texture-analysis-aided diagnosis provides higher sensitivity without loss of specificity on CT in

characterizing benign ovarian cysts. This additional diagnostic value is especially important for less trained radiologists. Not surprisingly, the abdominal radiologist outperformed the radiology resident in the detection of mucinous cystadenoma through classic interpretation. In this study, the expert radiologist demonstrated a slightly higher sensitivity than the previously reported 62% CT detection rate for mucinous cystadenomas (9). In contrast, the trainee initially diagnosed mucinous cystadenoma very conservatively, demonstrating far lower sensitivity and slightly higher specificity than the expert. With the addition of both decision trees, there were no significant changes in the sensitivity and specificity of the expert's diagnosis. However, after using both decision trees and texture analysis, the trainee's diagnostic sensitivity increased significantly. The improved sensitivity was even higher than the previously reported 70% MRI detection rate while preserving the specificity (10). The increased sensitivity was also significantly higher ($p = 0.001$) than that of the expert's conventional inter-

Table 4. Comparison of texture analysis parameters among four pathologic categories of ovarian cysts

		Simple or follicular cyst	Serous cystadenoma	Mucinous cystadenoma	Endometriotic cyst	<i>p</i>
Reviewer 1	SSF0, Mean	15.0 (5.2, 39.0)	11.9 (9.1, 18.4)*	19.9 (14.8, 25.1)	33.0 (26.2, 28.9)*	<0.001
	SSF0, MPP	20.1 (14.1, 44.9)	20.3 (16.3, 24.0)*	24.4 (19.4, 31.1)	35.6 (27.7, 41.5)*	<0.001
	SSF0, Skewness	0.3 (0, 0.5)	0.2 (0.0, 0.3)*	0.4 (0.1, 0.5)	0.3 (0.2, 0.7)	0.048
	SSF0, Kurtosis	1.5 (0.4, 1.8)	0.4 (0.2, 1.0)*	0.9 (0.3, 1.6)	0.7 (0.4, 1.3)	0.040
	SSF2, Mean	-2.4 (-6.1, 2.5)	-1.5 (-5.7, -0.5)*	-0.5 (-1.7, 0.7)	-3.3 (-6.0, -1.4)*	<0.001
	SSF2, Skewness	-0.1 (-0.3, 0.1)*	-0.1 (-0.4, 0.1)*	0.1 (0, 0.3)	0.1 (-0.1, 0.2)	0.001
	SSF3, Mean	-4.0 (-9.0, 3.5)	-3.3 (-9.7, -0.9)*	-1.6 (-4.2, -0.1)	-5.8 (-11.2, -2.5)*	0.002
	SSF3, SD	39.5 (30.1, 57.8)	37.0 (28.9, 43.5)	34.8 (28.6, 42.9)	42.4 (35.3, 49.0)*	0.029
	SSF3, Skewness	-0.2 (-1.0, 0.1)*	-0.4 (-0.9, 0.2)*	0.1 (-0.3, 0.4)	0 (-0.2, 0.4)	0.010
	SSF4, Mean	-6.3 (-13.0, 2.8)	-5.1 (-13.7, -1.7)	-2.9 (-7.0, -1.1)	-8.9 (-16.7, -4.7)*	0.006
	SSF4, SD	37.8 (30.0, 59.5)	34.1 (27.5, 42.1)	33.3 (26.4, 41.3)	43.3 (34.9, 51.4)*	0.006
	SSF4, Entropy	4.8 (4.6, 5.1)	4.8 (4.5, 5.1)	4.8 (4.5, 5.0)	5.0 (4.8, 5.2)*	0.007
	SSF4, MPP	17.8 (13.3, 35.8)	18.7 (15.0, 24.5)	22.9 (16.5, 28.7)	26.5 (20.8, 30.8)*	0.005
	SSF4, Skewness	-0.4 (-1.3, 0.4)	-0.8 (-1.7, 0.1)*	-0.1 (-0.6, 0.4)	0 (-0.5, 0.4)	0.017
	SSF5, Mean	-9.9 (-17.1, -0.3)	-6.7 (-18.0, -2.8)	-4.9 (-9.7, -2.2)	-11.3 (-20.9, -6.2)*	0.008
	SSF5, SD	39.3 (30.4, - 66.6)	33.3 (27.4, 43.3)	33.5 (28.2, 40.6)	44.7 (35.6, 54.9)*	0.001
	SSF5, Entropy	4.8 (4.5, 5.2)	4.7 (4.5, 5.0)	4.7 (4.5, 5.0)	5.1 (4.8, 5.2)*	0.001
	SSF5, MPP	13.8 (11.7, 35.0)	18.7 (13.0, 23.7)	20.8 (14.8, 28.4)	25.8 (20.5, 31.4)*	0.001
	SSF6, Mean	-14.0 (-21.3, -1.7)	-8.4 (-22.5, -3.8)	-7.2 (-12.1, -3.1)	-15.0 (-28.6, -8.6)*	0.009
	SSF6, SD	39.5 (31.9, 76.1)	35.7 (26.5, 42.8)	33.8 (28.8, 42.8)	47.9 (37.6, 60.4)*	<0.001
SSF6, Entropy	4.8 (4.6, 5.3)	4.7 (4.5, 5.0)	4.7 (4.5, 5.0)	5.1 (4.8, 5.2)*	0.001	
SSF6, MPP	12.9 (10.9, 35.6)	17.8 (1.8, 23.0)	20.0 (14.3, 28.5)	25.9 (20.5, 35.5)*	0.002	
Reviewer 2	SSF0, Mean	17.0 (7.6, 41.0)	12.3 (9.8, 23.1)*	20.4 (13.9, 24.4)	36.7 (29.0, 42.3)*	<0.001
	SSF0, SD	17.4 (15.9, 26.1)	17.8 (16.1, 21.7)	18.2 (15.7, 21.1)	20.5 (17.8, 26.1)*	0.038
	SSF0, MPP	24.0 (15.4, 46.6)	21.4 (16.6, 26.8)	24.2 (18.5, 30.1)	38.2 (31.8, 44.7)*	<0.001
	SSF2, SD	45.5 (38.3, 56.0)	42.6 (36.8, 53.1)	41.7 (37.6, 48.9)	48.1 (43.7, 59.3)*	0.006
	SSF2, Entropy	5.1 (5.0, 5.4)	5.1 (5.0, 5.3)	5.1 (5.0, 5.2)	5.2 (5.1, 5.4)*	0.010
	SSF2, MPP	34.7 (29.1, 44.9)	32.2 (27.7, 40.7)	32.4 (28.0, 37.7)	36.5 (33.1, 45.6)*	0.005
	SSF3,SD	40.6 (32.0 , 58.7)	37.8 (27.7, 45.6)	35.4 (29.2, 43.1)	46.4 (39.0, 50.9)*	0.001
	SSF3, Entropy	5.0 (4.7, 5.2)	4.9 (4.7, 5.1)	4.9 (4.7, 5.1)	5.1 (5.0, 5.2)*	0.001
	SSF3, MPP	25.3 (19.5, 36.8)	26.3 (20.0, 29.6)	25.7 (20.2, 32.1)	32.7 (28.6, 38.2)*	<0.001
	SSF4, SD	43.7 (32.7, 60.7)*	36.5 (25.1, 47.0)	33.4 (27.7, 41.1)	47.4 (38.3, 54.0)*	<0.001
	SSF4, Entropy	5.0 (4.6, 5.2)	4.8 (4.5, 5.1)	4.8 (4.5, 5.0)	5.1 (5.0, 5.2)*	<0.001
	SSF4, MPP	20.5 (14.9, 34.8)	21.9 (17.7, 26.1)	21.8 (17.0, 29.0)	31.3 (26.0, 37.6)*	<0.001
	SSF5, SD	45.7 (32.3, 72.6)*	38.3 (25.4, 45.9)	33.6 (28.4, 40.4)	50.9 (39.2, 55.5)*	<0.001
	SSF5, Entropy	5.0 (4.5, 5.3)	4.8 (4.5, 5.1)	4.7 (4.5 , 5.0)	5.1 (4.9, 5.3)*	<0.001
	SSF5, MPP	18.5 (13.3, 37.1)	19.1 (15.1, 25.3)	19.7 (15.5, 27.9)	33.4 (24.8, 37.9)*	<0.001
	SSF6, SD	47.6 (31.9, 84.2)*	40.0 (25.7, 45.7)	33.9 (28.2, 41.2)	51.8 (40.6, 63.9)*	<0.001
	SSF6, Entropy	5.0 (4.6, 5.4)*	4.7 (4.4, 5.1)	4.7 (4.5, 5.0)	5.2 (4.9, 5.3)*	<0.001
SSF6, MPP	18.0 (12.0 , 43.7)	18.4 (13.8, 27.0)	18.3 (14.1, 26.5)	33.3 (24.8, 38.3)*	<0.001	

Values are expressed as median (interquartile range).

*Parameters with clinically significant difference from mucinous cystadenoma.

SSF, spatial scaling factor; SD, standard deviation; MPP, mean of the positive pixels.

Table 5. Comparison of the diagnostic performance of each radiologist with and without the decision trees

		Sensitivity	Specificity	Positive predictive value	Negative predictive value	Accuracy	p^* (sensitivity)	p^* (specificity)
Reviewer 1	Radiologist's interpretation	68.1 (30/44)	80.2 (73/91)	62.5 (30/48)	83.9 (73/87)	76.3 (103/135)	-	-
	The 1 st decision tree	81.8 (36/44)	71.4 (65/91)	58.1 (36/62)	89.0 (65/73)	74.8 (101/135)	0.146	0.169
	The 2 nd decision tree	63.6 (28/44)	85.7 (78/91)	68.3 (28/41)	83.0 (78/94)	78.5 (106/135)	0.791	0.383
Reviewer 2	Radiologist's interpretation	31.8 (14/44)	89.0 (81/91)	58.3 (14/24)	73.0 (81/111)	70.4 (95/135)	0.001	0.096
	The 1 st decision tree	86.4 (38/44)	65.9 (60/91)	55.1 (38/69)	90.9 (60/66)	72.6 (98/135)	<0.001	<0.001
	The 2 nd decision tree	72.7 (32/44)	89.0 (81/91)	76.2 (32/42)	87.1 (81/93)	83.7 (113/135)	0.001	1.000

* Reference: reviewer 1's interpretation.

pretation. Therefore, the decision trees and texture analysis were able to compensate for the experience difference between a resident and an expert.

Adnexal lesions are sometimes incidentally found on abdominal-pelvic CT images that are obtained for other reasons, owing to the widespread use of CT (5). Additionally, a symptomatic ovarian cyst presents with nonspecific symptoms such as lower abdominal distension, pain, or urinary symptoms, often initially detected on CT. However, CT is not as commonly used in the specific diagnosis of benign adnexal mass lesions, resulting in a paucity of literature regarding the characteristic CT findings of common benign adnexal lesions (20, 21, 23–29). Although some radiologic findings can suggest a specific diagnosis, the CT appearance of adnexal cysts is nonspecific. This makes it very difficult to specifically characterize the type of cyst. We found a few conventional features that were effective in differentiating mucinous cystadenoma from other cysts.

Four conventional qualitative features, including septum number, septum thickness, locule number, and margin, were significantly different between mucinous cystadenomas and other cysts in both reviewers' analyses. These features are consistent with the known multilocular and complex cystic nature of mucinous cystadenomas. Bilateral ovarian involvement was more frequent in endometriotic cysts than in mucinous cystadenomas. The typical finding of mucinous cystadenomas on MRI is variable signal intensity in the locules. However, mucinous cystadenomas more commonly had homogeneous internal densities on CT in our study. Interestingly, calcifications were more frequently noted in mucinous cystadenomas than in serous cystadenomas according to reviewer 1. This finding is inconsistent with prior published data (11).

In the texture analysis, the mean, SD, and entropy values tended to be higher in endometriotic cysts than in mucinous cystadenomas. SD represents how the Hounsfield unit (HU) values are dispersed, and entropy represents the irregularity of its distribution. Mean and MPP (the mean HU of the pixels above zero) were highest in endometriotic cysts among all lesions. Endometriotic cysts may contain internal hemorrhage or blood clots, which results in higher overall density and intralocular heterogeneity (7, 26). By visual assessment, both reviewers also noticed more heterogeneity and higher density in endometriotic cysts than in mucinous cystadenoma. However, these differences were not significant according to reviewer 1. The texture analysis provided more objective and quantitative results by analyzing the mean and distribution (i.e., SD and entropy) of the Hounsfield units, revealing a significant difference between the two cysts according to both reviewers. These results ensure the clinical utility of texture analysis in evaluating the internal contents of adnexal masses, diagnosing its pathologic type, and eventually planning for treatment. Additionally, some parameters related to cyst density (mean and MPP) were significantly higher in mucinous cystadenomas than in serous cystadenomas.

Several recent articles have discussed the application of texture analysis to radiologic images of ovarian cancers. One study used texture-based analysis on US imaging to differentiate ovarian masses into functional cysts, dermoid cysts, or malignant tumors (30). Several other researchers have reported the texture analysis characteristics of ovarian malignancies, either by using MRI or CT as source images (17–19, 31). However, there is no study regarding the application of texture analysis in the diagnosis of benign ovarian cysts. To our knowledge, our study is the first to do so with a specific

focus on CT imaging. Our findings suggest that texture analysis can help to diagnose ovarian cysts with ambiguous CT findings.

Our study has several limitations. This was a retrospective study that was not randomized. Therefore, there was a risk of selection bias. In addition, the extrahospital CT images may have been obtained using different protocols, which could have contributed to the interexamination heterogeneity of texture, especially at SSF0. However, all CT images from outside hospitals were acceptable for diagnosis. Finally, there were only a few parameters that were significantly different between simple or follicular cysts and mucinous cystadenomas. Therefore, further studies are required to validate the utility and reproducibility of texture analysis.

In conclusion, this study suggests that the addition of texture analysis to conventional image analysis is helpful in differentiating mucinous cystadenomas from other benign adnexal cysts. This is particularly true for less experienced radiologists.

Conflict of interest disclosure

The authors declared no conflicts of interest.

References

- Spencer JA, Ghattamaneni S. MR imaging of the sonographically indeterminate adnexal mass. *Radiology* 2010; 256:677–694. [\[Crossref\]](#)
- Foti PV, Attina G, Spadola S, et al. MR imaging of ovarian masses: classification and differential diagnosis. *Insights Imaging* 2016; 7:21–41. [\[Crossref\]](#)
- Park SB, Lee JB. MRI features of ovarian cystic lesions. *J Magn Reson Imaging* 2014; 40:503–515. [\[Crossref\]](#)
- Masch WR, Daye D, Lee SI. MR imaging for incidental adnexal mass characterization. *Magn Reson Imaging Clin N Am* 2017; 25:521–543. [\[Crossref\]](#)
- Pickhardt PJ, Hanson ME. Incidental adnexal masses detected at low-dose unenhanced CT in asymptomatic women age 50 and older: implications for clinical management and ovarian cancer screening. *Radiology* 2010; 257:144–150. [\[Crossref\]](#)

6. Boos J, Brook OR, Fang J, Brook A, Levine D. Ovarian cancer: prevalence in incidental simple adnexal cysts initially identified in CT examinations of the abdomen and pelvis. *Radiology* 2018; 286:196–204. [\[Crossref\]](#)
7. Bennett GL, Harvey WB, Slywotzky CM, Birnbaum BA. CT of the acute abdomen: gynecologic etiologies. *Abdom Imaging* 2003; 28:416–432. [\[Crossref\]](#)
8. Togashi K. MR imaging of the ovaries: normal appearance and benign disease. *Radiol Clin North Am* 2003; 41:799–811. [\[Crossref\]](#)
9. Buy JN, Ghossain MA, Scioc C, et al. Epithelial tumors of the ovary: CT findings and correlation with US. *Radiology* 1991; 178:811–818. [\[Crossref\]](#)
10. Ghossain MA, Buy JN, Ligneres C, et al. Epithelial tumors of the ovary: comparison of MR and CT findings. *Radiology* 1991; 181:863–870. [\[Crossref\]](#)
11. Jung SE, Lee JM, Rha SE, Byun JY, Jung JI, Hahn ST. CT and MR imaging of ovarian tumors with emphasis on differential diagnosis. *Radiographics* 2002; 22:1305–1325. [\[Crossref\]](#)
12. Sagiv R, Golan A, Glezerman M. Laparoscopic management of extremely large ovarian cysts. *Obstet Gynecol* 2005; 105:1319–1322. [\[Crossref\]](#)
13. Shindholimath VV, Jyoti SG, Patil KV, Ammanagi AS. Laparoscopic management of large ovarian cysts at a rural hospital. *J Gynecol Endosc Surg* 2009; 1:94–97. [\[Crossref\]](#)
14. Mittal S, Gupta N, Sharma AK, Dadhwal V. Laparoscopic management of a large recurrent benign mucinous cystadenoma of the ovary. *Arch Gynecol Obstet* 2008; 277:379–380. [\[Crossref\]](#)
15. Lim S, Lee KB, Chon SJ, Park CY. Is tumor size the limiting factor in a laparoscopic management for large ovarian cysts? *Arch Gynecol Obstet* 2012; 286:1227–1232. [\[Crossref\]](#)
16. Vlahos NF, Iavazzo C, Marcopoulos MC, et al. Laparoscopic management of large ovarian cysts. *Surg Innov* 2012; 19:370–374. [\[Crossref\]](#)
17. Vargas HA, Veeraraghavan H, Micco M, et al. A novel representation of inter-site tumour heterogeneity from pre-treatment computed tomography textures classifies ovarian cancers by clinical outcome. *Eur Radiol* 2017; 27:3991–4001. [\[Crossref\]](#)
18. Rizzo S, Botta F, Raimondi S, et al. Radiomics of high-grade serous ovarian cancer: association between quantitative CT features, residual tumour and disease progression within 12 months. *Eur Radiol* 2018; 28:4849–4859. [\[Crossref\]](#)
19. Meier A, Veeraraghavan H, Nougaret S, et al. Association between CT-texture-derived tumor heterogeneity, outcomes, and BRCA mutation status in patients with high-grade serous ovarian cancer. *Abdom Radiol (NY)* 2019; 44:2040–2047. [\[Crossref\]](#)
20. Tsili AC, Dalkalitsis N, Paraskevaidis E, Tsampoulas K. Multi-detector CT features of benign adnexal lesions. *Acad Radiol* 2010; 17:31–38. [\[Crossref\]](#)
21. Borders RJ, Breiman RS, Yeh BM, Qayyum A, Coakley FV. Computed tomography of corpus luteal cysts. *J Comput Assist Tomogr* 2004; 28:340–342. [\[Crossref\]](#)
22. Dean CB, Nielsen JD. Generalized linear mixed models: a review and some extensions. *Lifetime Data Anal* 2007; 13:497–512. [\[Crossref\]](#)
23. Fishman EK, Scatarige JC, Saksouk FA, Rosen-shein NB, Siegelman SS. Computed tomography of endometriosis. *J Comput Assist Tomogr* 1983; 7:257–264. [\[Crossref\]](#)
24. Sawyer RW, Vick CW, Walsh JW, McClure PH. Computed tomography of benign ovarian masses. *J Comput Assist Tomogr* 1985; 9:784–789. [\[Crossref\]](#)
25. Fukuda T, Ikeuchi M, Hashimoto H, et al. Computed tomography of ovarian masses. *J Comput Assist Tomogr* 1986; 10:990–996. [\[Crossref\]](#)
26. Buy JN, Ghossain MA, Mark AS, et al. Focal hyperdense areas in endometriomas: a characteristic finding on CT. *AJR Am J Roentgenol* 1992; 159:769–771. [\[Crossref\]](#)
27. Bazot M, Ghossain MA, Buy JN, et al. Fibrothecomas of the ovary: CT and US findings. *J Comput Assist Tomogr* 1993; 17:754–759. [\[Crossref\]](#)
28. Shin YM, Lee JK, Turan N, Mauro D, Chong W. Computed tomography appearance of ovarian cysts with hyperenhancing rim during the menstrual cycle in women of different ages. *J Comput Assist Tomogr* 2010; 34:532–536. [\[Crossref\]](#)
29. Zhao Y, Mao X, Yao L, Shen J. Computed tomography imaging features of benign ovarian Brenner tumors. *Oncol Lett* 2018; 16:1141–1146. [\[Crossref\]](#)
30. Faschingbauer F, Beckmann MW, Weyert Goecke T, et al. Automatic texture-based analysis in ultrasound imaging of ovarian masses. *Ultraschall Med* 2013; 34:145–150. [\[Crossref\]](#)
31. Wang F, Wang Y, Zhou Y, et al. Comparison between types I and II epithelial ovarian cancer using histogram analysis of monoexponential, biexponential, and stretched-exponential diffusion models. *J Magn Reson Imaging* 2017; 46:1797–1809. [\[Crossref\]](#)